

Genetic and environmental circadian disruption induce weight gain through changes in the gut microbiome



Baraa Altaha^{1,2}, Marjolein Heddes^{1,2}, Violetta Pilorz³, Yunhui Niu^{1,2}, Elizaveta Gorbunova^{1,2}, Michael Gigl⁴, Karin Kleigrewe⁴, Henrik Oster³, Dirk Haller^{1,2}, Silke Kiessling^{1,2,5,*}

ABSTRACT

Objective: Internal clocks time behavior and physiology, including the gut microbiome, in a circadian (~24 h) manner. Mismatch between internal and external time, e.g. during shift work, disrupts circadian system coordination promoting the development of obesity and type 2 diabetes (T2D). Conversely, body weight changes induce microbiota dysbiosis. The relationship between circadian disruption and microbiota dysbiosis in metabolic diseases, however, remains largely unknown.

Methods: Core and accessory clock gene expression in different gastrointestinal (GI) tissues were determined by qPCR in two different models of circadian disruption - mice with *Bmal1* deficiency in the circadian pacemaker, the suprachiasmatic nucleus (*Bmal1^{SCNfl/-}*), and wild-type mice exposed to simulated shift work (SSW). Body composition and energy balance were evaluated by nuclear magnetic resonance (NMR), bomb calorimetry, food intake and running-wheel activity. Intestinal permeability was measured in an Ussing chamber. Microbiota composition and functionality were evaluated by 16S rRNA gene amplicon sequencing, PICRUSt2.0 analysis and targeted metabolomics. Finally, microbiota transfer was conducted to evaluate the functional impact of SSW-associated microbiota on the host's physiology.

Results: Both chronodisruption models show desynchronization within and between peripheral clocks in GI tissues and reduced microbial rhythmicity, in particular in taxa involved in short-chain fatty acid (SCFA) fermentation and lipid metabolism. In *Bmal1^{SCNfl/-}* mice, loss of rhythmicity in microbial functioning associates with previously shown increased body weight, dysfunctional glucose homeostasis and adiposity. Similarly, we observe an increase in body weight in SSW mice. Germ-free colonization experiments with SSW-associated microbiota mechanistically link body weight gain to microbial changes. Moreover, alterations in expression of peripheral clock genes as well as clock-controlled genes (CCGs) relevant for metabolic functioning of the host were observed in recipients, indicating a bidirectional relationship between microbiota rhythmicity and peripheral clock regulation.

Conclusions: Collectively, our data suggest that loss of rhythmicity in bacteria taxa and their products, which likely originates in desynchronization of intestinal clocks, promotes metabolic abnormalities during shift work.

© 2022 The Authors. Published by Elsevier GmbH. This is an open access article under the CC BY license (<http://creativecommons.org/licenses/by/4.0/>).

Keywords Circadian rhythm; SCN; Shift work; Microbiota; Short chain fatty acids; Bile acids

1. INTRODUCTION

Most species have evolved endogenous circadian clocks to facilitate adaption to daily recurring changes. A complex hierarchical circadian system consists of a central clock in the suprachiasmatic nuclei (SCN) of the hypothalamus which regulates rhythmic behavior, such as rest-activity, and synchronizes peripheral clocks via neuronal and humoral signals to adapt to environmental changes [1]. Peripheral circadian clocks have been identified in various organs, including the gastrointestinal (GI) tract, and regulate tissue-specific functions, such as glucocorticoid synthesis and glucose metabolism [2,3]. On the

molecular level, the circadian clock consists of a subset of interconnected clock genes which regulate circadian rhythms of tissue-specific clock-controlled genes (CCGs) and thereby control various aspects of physiology [4].

Mismatch between the internal clock and the environmental time, observed in shift workers, induces circadian desynchronization among peripheral clocks [5]. Genetically and environmentally induced circadian disruption has been associated with various metabolic and GI diseases including obesity and diabetes [6–8]. Similarly, lack of the coordinative input from the central clock results in desynchronization between peripheral clocks and causes an increase in body weight and

¹ZIEL - Institute for Food & Health, Technical University of Munich, Gregor-Mendel Str. 2, 85354 Freising, Germany ²Chair of Nutrition and Immunology, Technical University of Munich, Gregor-Mendel-Str. 2, 85354 Freising, Germany ³Institute of Neurobiology, Center of Brain, Behavior & Metabolism, University of Lübeck, Marie Curie Street, 23562, Lübeck, Germany ⁴Bavarian Center for Biomolecular Mass Spectrometry, Technical University of Munich, Gregor-Mendel-Str. 4, 85354 Freising, Germany ⁵Faculty of Health and Biomedical Science, University of Surrey, 388 Stag Hill Campus, GU27XH, Guildford, UK

*Corresponding author. Chair of Nutrition and Immunology Technical University of Munich Gregor-Mendel-Str. 2 85354 Freising, Germany. E-mail: silke.kiessling@tum.de (S. Kiessling).

Received July 19, 2022 • Revision received October 29, 2022 • Accepted October 30, 2022 • Available online 2 November 2022

<https://doi.org/10.1016/j.molmet.2022.101628>

Abbreviations

BA	bile acid	LD	12 h light and 12 h darkness schedule
<i>Bmal1</i>	Brain and Muscle ARNT-Like 1	LEFSE	LDA effective score
CCGs	clock-controlled genes	NMR	Nuclear magnetic resonance
<i>Cry1</i>	cryptochrome circadian regulator 1	<i>Per2</i>	Period 2
CT	circadian time	PICRUST	Phylogenetic Investigation of Communities by Reconstruction of Unobserved States
<i>Dbp</i>	D Site of Albumin Promoter (Albumin D-Box) Binding Protein	<i>Pparγ</i>	Peroxisome Proliferator Activated Receptor Gamma
DD	constant darkness	qRT-PCR	Quantitative real-time PCR
EC	Enzyme Commission	<i>Rev-erbα</i>	Nuclear receptor subfamily 1 group D member 1
<i>Ef1a</i>	Elongation factor 1-alpha	SCFA	short-chain fatty acid
<i>Fabp2</i>	Fatty Acid Binding Protein 2	SCN	suprachiasmatic nucleus
GF	Germ-free	SPF	specific-pathogen free
GI	gastrointestinal	SSW	simulated shift work
GUniFrac	Generalized UniFrac	T2D	type 2 diabetes
<i>Glut2</i>	Glucose transporter 2	UPL	Universal Probe Library system
<i>Hdac3</i>	Histone Deacetylase 3	zOTUs	Zero-radius operational taxonomic units
<i>Ifabp</i>	Intestinal-type fatty acid-binding protein	ZT	<i>Zeitgeber</i> time

impaired glucose tolerance [6,9]. These results suggest that peripheral circadian desynchronization might be causal for metabolic alterations. In the context of metabolic disease, human cohort studies have identified altered microbial profiles associated with obesity, insulin resistance, and T2D [10–14]. In agreement with these findings, frequent time zone shifts (jetlag) induce major alterations in overall gut microbiota communities and loss of daytime-dependent oscillation in specific taxa [15]. Importantly, in large human cohorts we showed that microbiota composition and function undergo 24-h rhythmicity and are disrupted in subjects with obesity and/or type 2 diabetes (T2D) [16]. Interestingly, our results in prediabetic patients indicate that arrhythmicity of specific taxa precedes the onset of diabetes and a signature of arrhythmic bacteria predicts T2D risk in populations. Of importance, our recent work on mice identified clocks in cells of the GI tract to be the major regulators of microbial rhythmicity and, therefore, GI homeostasis [17]. Consequently, we hypothesize that intestinal clock-controlled oscillation of the microbiome provides a functional link to metabolic requirements of the host to maintain metabolic health.

Here we investigate the impact of circadian disruption on the synchronization of GI clocks and the rhythmicity of microbiota composition and function. Our results show desynchronization of GI clocks in two independent models of circadian disruption, a genetic approach using mice with central circadian dysfunction and an environmental approach using simulated shift work (SSW) on wild type mice. Arrhythmicity of microbial taxa was observed in both models, although microbiota composition differed between experiments. Importantly, arrhythmic bacterial taxa and metabolites identified in both models shared functionalities relevant for metabolic homeostasis of the host. Microbiota transfer further revealed a cross-talk between oscillating taxa and intestinal clocks, highlighting the physiological relevance of microbial rhythms for metabolic health and as therapeutic target.

2. MATERIAL AND METHODS

2.1. Ethics statement

Experiments were conducted at Technical University of Munich in accordance with Bavarian Animal Care and Use Committee (TVA ROB-55.2Vet-2532. Vet_02-18-14) or were conducted at the University of Lübeck licensed by the Ministry of Agriculture, Environment and Rural Areas (MELUR) of the state of Schleswig–Holstein (project license:42-5/18_Oster).

2.2. Mouse models and light conditions

2.2.1. *Syt10^{cre}-Bmal1^{IEC} +/-* and *Syt10^{cre}-Bmal1^{IECfl/-}* mice

Male SCN-specific *Bmal1* knock-out (Synaptotagmin-10 CRE/wt x *Bmal1^{fl/-}*; referred to as *Bmal1^{SCNfl/-}*) mice and their control littermates (Synaptotagmin-10 CRE/wt x *Bmal1^{+/-}*; referred to as *Bmal1^{SCN+/-}*) on a genetic C57BL/6J background, mice were generated at the University of Lübeck as described before [18]. Male mice were maintained under a 12 h light and 12 h darkness schedule (LD) cycle for 2 weeks (age 8–10 weeks), and sacrificed at the indicated time points during the 2nd day in constant darkness (DD).

2.2.2. Simulated shift work (SSW)

Wild type mice on a genetic C57BL/6J background were bred in house at the Technical University of Munich. Male mice were kept in LD 12:12 cycles (300 lux), with lights turned on at 5am (*Zeitgeber* time (ZT0) to 5pm (ZT12)). Mice were single housed at the age of 8 weeks in running wheel-equipped cages with ad libitum access to chow and water and under specific-pathogen free (SPF) conditions according to the FELASA recommendation. To minimize cage-related bias in microbiota composition [19], littermates and litters of comparable age from as few as possible breeding pairs and cages were selected. One set of control males was maintained under a LD cycle for 8 weeks (age 8–16 weeks), whereas another set of male mice was first exposed to for 2 weeks (age 8–10 weeks) of LD and then subjected to SSW conditions for at least 6 weeks. During the experiment mice were exposed to 100 lux light intensity and shifted every 5th day by 8 h. On day 1 of the jet lag, the lights-off time (ZT12) was shifted from 5 pm to 9 am (phase advance paradigm) and from 9 am to 5 pm (phase delay paradigm). Using a short day protocol, we defined day 1 as the first advanced dark period as defined previously [5].

2.2.3. Behavior analysis

Running-wheel activity was analyzed with ClockLab software (v6.0.52, Actimetrics). We assessed individual mice activity onset using ClockLab Analysis software and confirmed each onset by visual inspection. Activity profiles were calculated based on the count of running wheel spins per 6 min. Total activity was calculated as the total counts of running wheel spins per day. We calculated the percentage of day/night activity by normalizing the activity during the day/night to the total activity per day.

2.2.4. Germ free colonization experiment transfer experiments

Germ-free wild type C57BL6 were gavaged at the age of 10 weeks with cecal microbiota from mixture of cecal content diluted 1:10 in 40% glycerol. Cecal microbiota of 4–5 mice sacrificed at ZT13 from LD and SSW group were adjusted to 7×10^6 bacteria/ μ l and 100 μ l were used for gavaging each mouse at ZT13. Germ free recipient mice kept in LD12:12 and were checked weekly for bodyweight changes. After 6 weeks of the gavage, at age 16 weeks, mice were released in constant darkness and sacrificed at the 2nd day at the indicated time point.

2.3. Food intake

For food intake profiling, mice were kept under 12:12 light–dark conditions (LD; 200 lux in the light phase) for one week and then released into constant darkness (DD). Feeding profiles were determined using the BioDAQ food intake monitor (Research Diets, New Brunswick, USA) and powdered normal chow. Data were collected in 1-hour bins. For LD, day-5 and -6 data were averaged. For DD, measurements were taken from 48 h after “lights off” for 24 h.

2.4. Tissue collection

All animals were sacrificed by cervical dislocation followed by decapitation at the age of 16–20 weeks. *Bmal1*^{SCN11/-} mice were sacrificed during the 2nd day of darkness at the indicated circadian time (CT) points. Control mice in the SSW experiment were sacrificed in LD conditions at the indicated *Zeitgeber* time (ZT) and animals undergoing SSW were sacrificed during the 1st day following the final phase advance of SSW at the indicated time point according to the LD control cohort. Tissues were collected and snap frozen using dry ice and stored in -80° until further processing.

2.5. Gut permeability

Gut permeability was measured using Ussing chambers as described previously [20–22]. Briefly, we took 1.5 cm of the proximal colon directly after dissecting the mice. The tissue was cut open and fixed as a flat sheet separating the two halved of the Ussing chamber (six chamber system - Scientific instruments). The tissue was supported from the two sides with carbogen-gassed freshly prepared Krebs buffer (5.4 mM KCl, 114 mM NaCl, 1.2 mM CaCl₂, 21 mM NaHCO₃, 1.2 mM MgCl₂, 2.4 mM Na₂HPO₄, 10 mM glucose, 0.6 mM NaH₂PO₄, pH 7.4) at 37 °C. We added 250 μ l of 1.7673 mM fluorescein to the luminal side, then we determined the fluorescence intensity at 45 and 60 min from the buffer on the serosal part, to calculate tissue permeability in cm/s.

2.6. Gene expression analysis (qRT-PCR) quantitative real-time PCR

Snap frozen tissue samples were used to extract RNA samples with Trizol reagent. Next we used 1000 ng RNA to synthesize cDNA with

probes to measure gene expression: Brain and Muscle ARNT-Like 1 (*Bmal1*) F 5'-ATTCCAGGGGAACCAGA- R 5'-GGCGATGACCCTCT-TATCC-3' Probe 15, Nuclear receptor subfamily 1 group D member 1 (*Rev-erba*) F 5'- AGGAGCTGGCCTATTAC-3' R 5'-CGGTCTTCAG-CACCAGAG-3' probe 1, Period 2 (*Per2*) F 5'-TCCGAGTATATCGTGAA-GAACG-3' R 5'- CAGGATCTTCCAGAAACCA-3' probe 5, D Site Of Albumin Promoter (Albumin D-Box) Binding Protein (*Dbp*) F 5'- ACAG-CAAGCCAAAGAACC-3' R 5'- GAGGGCAGAGTTGCCCTTG-3' probe 94, (*Cry1*) F 5'- ATCGTGCGCATTTCACATAC-3' R 5'- TCCGCCATTGAGTTC-TATGAT-3' probe 85, Glucose transporter 2 (*Glut2*) F 5'-TTACCGA-CAGCCATCCT-3' R 5'-TGAAAAATGCTGGTTGAATAGTAAAA-3' probe 3, Fatty Acid Binding Protein 2 (*Fabp2*) F 5'- ACGGAACGGAGCTCACTG-3' R 5'- TGGATTAGTTCATTACCAGAAACCT-3' probe 56, Peroxisome Proliferator Activated Receptor Gamma (*Pparg*) F 5'- AAGACAACGGA-CAAATACCA-3' R 5'- GGGGGTGATATGTTGAACCTG-3' probe 7, Histone Deacetylase 3 (*HDAC3*) F 5'- GAGAGTCCCGAGGAGAAC-3' R 5'- CGCCATCATAGAACTCATTGG-3' probe 40, Intestinal-type fatty acid-binding protein (*Ifabp*) 5'-GGTTTCTGGTAATGAACTAATCCAG-3' 5'- AAATCTGACATCAGCTTAGCTCTTC-3' probe 1, the housekeeping gene Elongation factor 1-alpha (*Ef1a*) F 5'- GCCAAT TTCTGGTTGGAATG-3' R 5'-GGTGACTTTCATCCCTTGA-3' probe 67 was used to normalize gene expression.

2.7. Nuclear magnetic resonance (NMR)

Body composition (fat, lean mass, free fluid) was measured using a minispec TD-NMR analyser (Bruker Optics, Ettlingen, Germany). Mice were placed in a plastic restrainer and inserted in the minispec for measurements.

2.8. Plasma glucose and triglycerides measurement

Non fasting fresh blood was collected directly after sacrificing the mice from the portal vein using 6% EDTA rinsed needle. To collect plasma, we centrifuged the blood at 4000 rcf for 10 min. Plasma samples were then stored at -80° C till further use. We measured plasma glucose and Triglycerides using Fluitest® GLU (analyticon, Germany) and Triglyceride gpo-pap (LT-SYS®, Germany), respectively, following the manufacture instruction.

2.9. Energy assimilation

Fecal samples were collected from individual mice over 5 days and dried at 55 °C for another 5 days. Dried fecal pellets were grinded using the TissueLyserII (Qiagen, Retsch, Haan, Germany) and pressed into pellets of 1 g (technical duplicates). Gross fecal energy content was measured using a 6400 calorimeter (Parr Instrument Company, Moline, IL, USA). Assimilation efficiency was calculated by recording the food intake and feces production over the fecal collection days as indicated in the formula below.

$$\text{Assimilation efficiency (\%)} = \frac{(\text{Food intake [g]} * \text{Efood [kJ*g}^{-1}]) - (\text{Feces production [g]} * \text{Efeces [kJ*g}^{-1}])}{\text{Food intake [g]} * \text{Efood [kJ*g}^{-1}]} * 100$$

cDNA synthesis kit Multiscribe RT (ThermoFischer Scientific). We performed qPCR in Light Cycler 480 system (Roche Diagnostics, Mannheim, Germany) using Universal Probe Library system (UPL) according to manufacturer's instructions. We used the following primers and

2.10. High-throughput 16S ribosomal RNA (rRNA) gene sequencing and microbial analysis

Snap-frozen fecal samples was processed in accordance to a slightly modified protocol from Godon and colleagues to isolate genomic DNA

[23]. DNA was purified with DNA NucleoSpin gDNA columns (Machery-Nagel, No. 740230.250). 24 ng DNA was used in a two-step PCR using 341F-ovh and 785r-ov primer to amplify V3–V4 region of 16s rRNA. Sampled were pooled and sequenced in pair-end mode (2×250 bp) on Illumina HiSeq using Rapid V2 chemistry, as previously described [16]. For every 45 samples we included two negative controls of DNA stabilizer without fecal samples to insure reproducibility and control for artifacts. High quality sequence of 16s rRNA with >500 read counts were used for microbial data analysis. FASTQ files were further processed with NGSToolkit (Version 3.5.2_64) with trim score of 5 at both 5' and 3' end of R1 and R2 read, then chimera was removed with FASTQ mergepair script of USEARCH. Zero-radius operational taxonomic units (zOTUs) were generated after denoising, deduplicating, clustering and merging quality filtered reads. Here we used zOTUs to have the utmost possible resolution of 16s rRNA sequencing by correcting for sequencing error and identifying sequence with 100% similarity as a unique microbial strain. Taxonomy was assigned based on EZBiocloud database, and RHEA pipeline was used to analyze the data. We aligned the sequence by the maximum likelihood approach with MUSCLE from the software MegaX to generate phylogenetic trees and use the online tool Evolview for tree visualization (<http://www.evolgenius.info/evolview>) [24]. For quantitative analysis, we add spike of 12 artificial DNA that mimics 16s rRNA genes in order to determine 16s rRNA genes copy numbers per gram of fecal sample as previously described [17].

2.11. PICRUST 2.0

Metagenomic functionality were predicted using PICRUST2.0. Briefly, based on zOTUs sequence metagenome was constructed to predict functional genes, Normalized zOTU copy numbers were multiplied by the genes for each zOTU. Finally, enzymatic genes were classified to Enzyme Commission (EC) numbers and were assigned to Metacyc pathways. After removing super-classes, we used Metacyc pathways for LDA effective score (LEFSE) calculation [25] using the online tool (<http://huttenhower.sph.harvard.edu/galaxy>).

2.12. Targeted bile acid (BA) and short chain fatty acid (SCFA) measurements

Samples were prepared and measured as described previously (Nature paper). Briefly, 20 mg fecal samples were extracted by bead beating (3 times of 20 s 6 m/s with 30 s breaks) with FastPrep-24 5G bead beating grinder (MP Biomedicals) supplied with a CoolPrep adapter. To measure BA and SCFAs, we used multiple reaction monitoring method and 3-NPH method, respectively, as described previously [26]. We used analyst 1.7 software (Sciex, Darmstadt, Germany) for data acquisition.

2.13. Statistical analysis

Statistical analysis was performed using GraphPad Prism, version 9.3.0 (GraphPad Software), R and online platforms (see below). The RHEA pipeline (Lagkouravdos) was used to calculate generalized Unifrac distances between sample and consequently to determine microbiota diversity, MDS plots were used to visualize distances between samples [27]. To calculate the circadian pattern of each 24h period graphs, we used cosine-wave equation: $y = \text{baseline} + (\text{amplitude} \cdot \cos(2 \cdot \pi \cdot ((x - [\text{phase shift}]/24))))$, with a fixed 24-h period. This equation was used to determine significance of rhythmicity of clock genes, richness, phyla, family and exemplatory profiles of zOTUs. Overall rhythmicity of zOTUs was determined with JTK_CYCLE algorithm [28]. For the manhattan plots JTK_CYCLE was used to calculate amplitude, p-value (p-

value = 1 were deleted for better visualization of the data) and the phase was calculated by cosine-wave regression. Evolview was used for tree visualization (<http://www.evolgenius.info/evolview>) [24]. To generate heatmaps with the online tool (heatmapr.ca) [29], we sorted the zOTUs or pathways based on the phase of the control group for visualization. The R package SIAMCAT with the function “check.-association” [30] was used to generate abundance plots. In order to compare two groups, the non-parametric Mann–Whitney test was used. Two-way ANOVA was used to compare weight gain, clock genes expression in SSW and transfer experiment with Tukey posthoc test for multiple comparison. P-values ≤ 0.05 were assumed as statistically significant.

3. RESULTS

3.1. Central clock dysfunction induces circadian desynchronization in the GI tract

Mice lacking a functional central clock display rhythmic food intake behavior in LD, albeit reduced in amplitude compared to WT (cosine wave regression: $p = 0.0403$, Figure 1A). Day-night differences in food intake are lost in *Bmal1^{SCN^{fl}/-}* mice when released into constant darkness (DD) (Figure 1A). Recently we showed that peripheral clocks such as the adrenal, liver, kidney, heart, pancreas, and white adipose tissue gradually desynchronize in these mice in DD [6,9]. As a consequence of system-wide circadian desynchronization, these mice develop obesity and altered glucose metabolism [6]. Of importance, metabolic homeostasis is partially controlled by GI functions regulated by the circadian system [31]. To investigate the degree of circadian desynchronization in peripheral clocks within the GI tract, we compared clock gene expression rhythms in the jejunum, cecum and proximal colon between mice lacking the major clock gene *Bmal1* specifically in the SCN (*Bmal1^{SCN^{fl}/-}*) and their littermate controls (*Bmal1^{SCN^{+/+}/-}*) on the 2nd day of DD (Figure 1, Table 1). Circadian rhythmicity analysis revealed that the expression of the core clock genes *Bmal1*, *Per2* and *Rev-erba* followed circadian oscillation in the jejunum in both genotypes (cosine-wave regression, control: $p = 0.004$, $p = 0.02$, $p = 0.03$, *Bmal1^{SCN^{fl}/-}*: $p = 0.01$, $p = 0.01$, $p = 0.04$) (Figure 1B, Table 1). However, the circadian phases in all clock genes examined in *Bmal1^{SCN^{fl}/-}* were significantly advanced (*Bmal1*: 2.7h, *Per2*: 3.6h, *Rev-erba*: 5.7h). In addition, the baseline of *Rev-erba* was reduced, *Dbp* did not show significant rhythmicity using cosine regression, but a significant time effect was found in both genotypes by two-way ANOVA analysis ($p = 0.01$). *Cry1* lost rhythmicity in *Bmal1^{SCN^{fl}/-}* mice (*Cry1*: $p = 0.009$, $p = 0.42$). In the cecum, all clock genes examined lost rhythmicity in *Bmal1^{SCN^{fl}/-}* mice, although a time effect was found for both genotypes by two-way ANOVA (time: *Bmal1* $p = 0.006$, *Per2* $p = 0.002$, *Rev-erba* $p = 0.0009$, *Dbp* $p = 0.03$, *Cry1* $p = 0.003$) (Figure 1C, Table 1). In contrast, rhythmicity of *Bmal1*, *Per2* and *Cry1* gene expression in the proximal colon was undistinguishable between genotypes, and the amplitude of *Rev-erba* expression was significantly reduced (cosine regression, $p = 0.02$). Similar to results obtained from jejunum, *Dbp* lost rhythmicity in *Bmal1^{SCN^{fl}/-}* mice (Figure 1D, Table 1). Altogether, these results suggest that in *Bmal1^{SCN^{fl}/-}* mice the jejunal clock free-runs with a reduced amplitude, the cecal clock slowly loses its functionality, whereas the colon clock is functional, albeit with a dampened amplitude. Consequently, these data demonstrate profound disruption of GI clocks in the absence of a functional central clock, which appears at a very early stage following release into constant darkness.

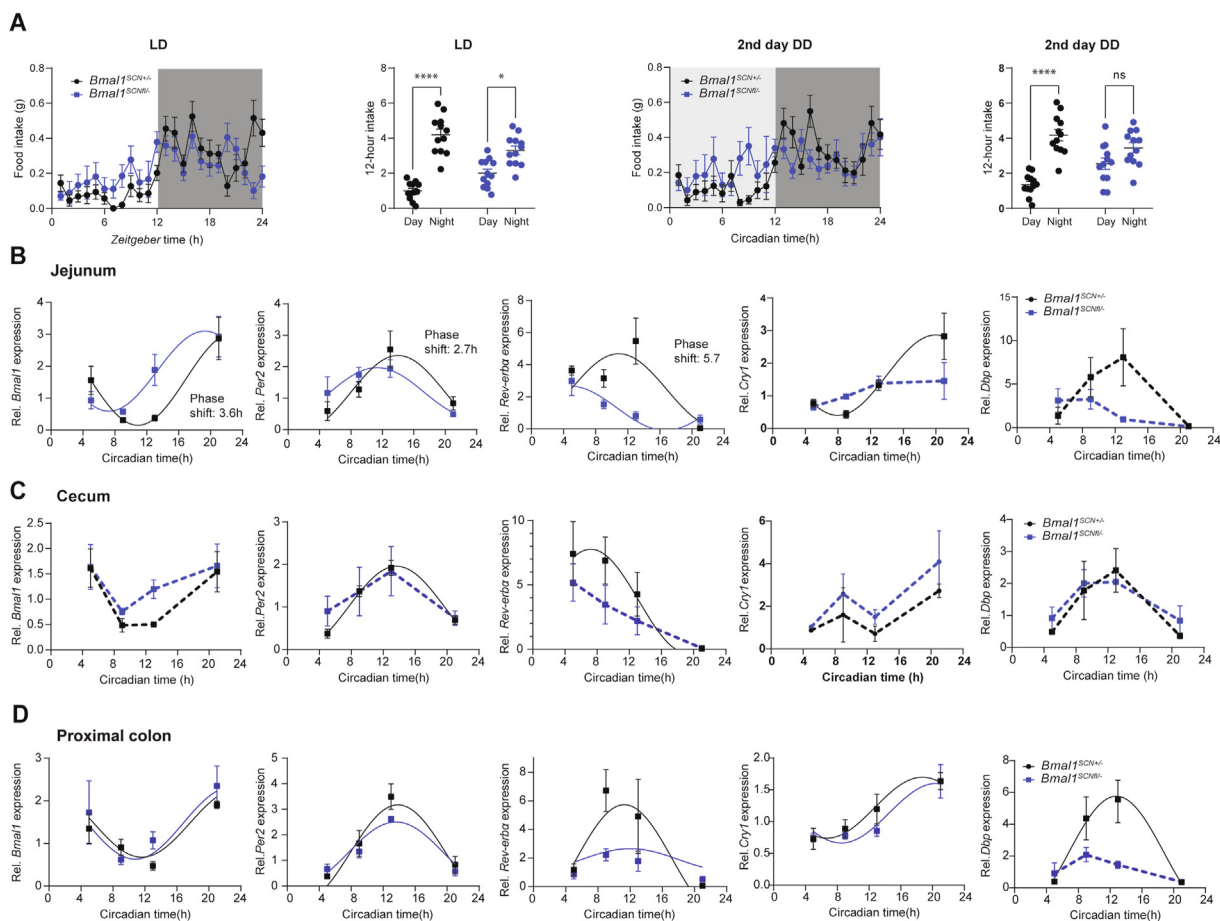


Figure 1: Central clock dysfunction induces circadian desynchronization in the GI tract. Feeding-fasting behavior of *Bmal1*^{SCN^{-/-} mice (blue) and their controls *Bmal1*^{SCN^{+/-} (black) in LD and the 2 days into DD. Relative expression of core and accessory clock genes in the jejunum (B), cecum (C), proximal colon (D) of *Bmal1*^{SCN^{-/-} mice (blue) and their controls *Bmal1*^{SCN^{+/-} (black). Significant rhythms according to cosine-wave regression analysis (p -value ≤ 0.05) are visualized with a solid line, while data connected by dashed line indicate arrhythmicity. Significant phase shifts ($p \leq 0.05$) are indicated with the number of hours of phase shift. $n = 3-4$ mice/time point/genotype. For food intake we used 12 mice per group/time/light condition. 2 Way-ANOVA used to assess the difference between group and day-night, P value * ≤ 0.05 , ** ≤ 0.01 , *** ≤ 0.001 , **** ≤ 0.0001 Data are represented as mean \pm SEM.}}}}

3.2. Disruption of microbiota rhythmicity in SCN-specific *Bmal1*-deficient mice

GI clocks and food intake are important regulators of circadian microbiome fluctuations and thereby balance GI homeostasis [15,17]. This prompted us to determine whether circadian desynchronization in *Bmal1*^{SCN^{-/-} mice affects circadian microbiota composition and function. Indeed, 16s rRNA analysis of fecal samples revealed significant clustering according to genotype (Figure 2A), suggesting a different microbiota composition in *Bmal1*^{SCN^{-/-} mice. Moreover, circadian rhythmicity in community diversity (species richness) observed in control mice was abolished in *Bmal1*^{SCN^{-/-} mice, although Generalized UniFrac distance (GUniFrac) quantification to CT1 identified a time difference in both genotypes (two-way ANOVA, $p = 0.0037$) (Figure 2B). Relative abundance of the two major phyla, *Firmicutes* and *Bacteroidetes*, showed circadian rhythmicity with similar patterns in both genotypes (Figure 2C). However, previous research, including from our own group, showed that rhythmicity in relative abundance can be masked due to oscillations of highly abundant taxa [17,32]. Thus, we used synthetic DNA spikes to determine quantitative microbiota composition as previously described [33]. Indeed, both phyla lost rhythmicity in quantitative}}}

abundance in *Bmal1*^{SCN^{-/-} mice compared to controls (Figure 2C). Central clock disruption led to loss of rhythmicity of the families *Lactobacillaceae* and *Clostridiales* independent of the analysis (Suppl. Figure S1A). Then we set out to determine rhythmicity of zero-radius OTUs (zOTUs) after removal of low-abundance taxa (mean relative abundance $< 0.1\%$; prevalence $< 10\%$). The heatmaps illustrate disrupted circadian oscillations of zOTUs in *Bmal1*^{SCN^{-/-} mice for both analyses (Figure 2D, Suppl. Figure 1B). The amount of rhythmic zOTUs was reduced by three quarters in mice with SCN-specific *Bmal1* deficiency, whereas only a few bacterial taxa gained rhythmicity (JTK_CYCLE, adj. p -value < 0.05) (Figure 2E, Suppl. Figure S1C, Suppl. Table. 1). For example, we identified zOTUs which lost rhythmicity in *Bmal1*^{SCN^{-/-} mice predominantly belonging to mucus foragers (*Muribaculaceae*) and to the secondary bile acid and SCFA producing family *Ruminococcaceae* [34,35] (Figure 2F, Suppl. Figure S1D). In particular, SCFA producing taxa, including *Faecalibaculum* and *Agathobaculum* [36], were arrhythmic in *Bmal1*^{SCN^{-/-} mice (Figure 2F,G, Suppl. Figure S1D,E). Of note, bacteria belonging to *Alloprevotella*, *Muribaculaceae* and *Faecalibaculum* lost rhythmicity and additionally differed in their abundance between genotypes (Suppl. Figure S1F).}}}}

Table 1 — Summary of results for phase, amplitude, baseline and rhythmicity of core and accessory clock gene expression based on cosine regression analysis in the GI tract of *Bmal1^{SCN^{fl}/-}* mice and control. Bold p-values indicate significant difference between genotype.

Gastrointestinal tissue	Gene	Group	Rhythmicity (P. value)	Phase shift (P. value)	Amplitude difference (P. value)	Baseline difference (P. value)
Jejunum	<i>Bmal1</i>	<i>Bmal1^{SCN+/+}</i>	0.004	0.02	0.64	0.42
		<i>Bmal1^{SCN^{fl}/-}</i>	0.01	Phase shift = 3.6		
	<i>Per2</i>	<i>Bmal1^{SCN+/+}</i>	0.02	0.04	0.28	0.83
		<i>Bmal1^{SCN^{fl}/-}</i>	0.01	Phase shift = 2.7		
	<i>Rev-erbα</i>	<i>Bmal1^{SCN+/+}</i>	0.03	0.03	0.28	0.04
		<i>Bmal1^{SCN^{fl}/-}</i>	0.04	Phase shift = 5.7		
	<i>Cry1</i>	<i>Bmal1^{SCN+/+}</i>	0.009	0.33	0.07	0.11
		<i>Bmal1^{SCN^{fl}/-}</i>	0.42			
	<i>Dbp</i>	<i>Bmal1^{SCN+/+}</i>	0.056	0.08	0.08	0.14
		<i>Bmal1^{SCN^{fl}/-}</i>	0.06			
Cecum	<i>Bmal1</i>	<i>Bmal1^{SCN+/+}</i>	0.06	0.53	0.34	0.3
		<i>Bmal1^{SCN^{fl}/-}</i>	0.33			
	<i>Per2</i>	<i>Bmal1^{SCN+/+}</i>	0.00006	0.54	0.37	0.59
		<i>Bmal1^{SCN^{fl}/-}</i>	0.31			
	<i>Rev-erbα</i>	<i>Bmal1^{SCN+/+}</i>	0.02	0.59	0.29	0.12
		<i>Bmal1^{SCN^{fl}/-}</i>	0.08			
	<i>Cry1</i>	<i>Bmal1^{SCN+/+}</i>	0.37	0.76	0.74	0.15
		<i>Bmal1^{SCN^{fl}/-}</i>	0.52			
	<i>Dbp</i>	<i>Bmal1^{SCN+/+}</i>	0.056	0.78	0.34	0.45
		<i>Bmal1^{SCN^{fl}/-}</i>	0.1			
Proximal colon	<i>Bmal1</i>	<i>Bmal1^{SCN+/+}</i>	0.01	0.53	0.67	0.22
		<i>Bmal1^{SCN^{fl}/-}</i>	0.04			
	<i>Per2</i>	<i>Bmal1^{SCN+/+}</i>	0.004	0.56	0.13	0.25
		<i>Bmal1^{SCN^{fl}/-}</i>	0.001			
	<i>Rev-erbα</i>	<i>Bmal1^{SCN+/+}</i>	0.03	0.98	0.02	0.07
		<i>Bmal1^{SCN^{fl}/-}</i>	0.03			
	<i>Cry1</i>	<i>Bmal1^{SCN+/+}</i>	0.01	0.27	0.94	0.47
		<i>Bmal1^{SCN^{fl}/-}</i>	0.01			
	<i>Dbp</i>	<i>Bmal1^{SCN+/+}</i>	0.008	0.39	0.002	0.04
		<i>Bmal1^{SCN^{fl}/-}</i>	0.07			

3.3. SCN clock-controlled microbial functions balance metabolic homeostasis

To address the potential physiological relevance of microbial rhythmicity we performed PICRUST 2.0 analysis on zOTUs which lost rhythmicity in *Bmal1^{SCN^{fl}/-}* mice [37]. SCN clock-deficient mice develop adiposity and impaired glucose handling [6]. In this context, genotype differences and loss of rhythmicity was observed in predicted pathways related to sugar metabolism, SCFA fermentation and fatty acid metabolism (Figure 3A, Suppl. Figure S2A). Targeted metabolite analysis further revealed that alterations in taxa identified in *Bmal1^{SCN^{fl}/-}* mice led to changes in key bacterial products involved in sugar and lipid signaling, such as SCFAs and BAs (Figure 3B–F, Suppl. Figure S2B–D). In particular, propionic acid, important for lipid metabolism [38], showed reduced levels in *Bmal1^{SCN^{fl}/-}* mice (Figure 3B). Moreover, branched-chain fatty acids including isovaleric acid, isobutyric acid and 2-methylbutyric acid were reduced in *Bmal1^{SCN^{fl}/-}* mice, whereas total SCFA concentrations were undistinguishable between genotypes (Figure 3B, Suppl. Figure S2B). Rhythmicity of total SCFAs as well as of major microbial derived products such as acetic acid, propionic acid and lactic acid was absent in *Bmal1^{SCN^{fl}/-}* mice (cosine regression, control: $p = 0.003$, $p = 0.001$, $p = 0.02$, $p = 0.0009$, *Bmal1^{SCN^{fl}/-}*: $p = 0.32$, $p = 0.5$, $p = 0.49$, $p = 0.93$) (Figure 3C). Of note, other SCFAs, including butyric acid and valeric acid, showed rhythmicity in both genotypes (cosine regression, control $p = 0.0001$, $p = 0.007$, *Bmal1^{SCN^{fl}/-}*, $p = 0.02$, $p = 0.01$, respectively) (Suppl. Figure S2C). In addition, BAs concentrations were altered in mice lacking a functional central clock (Figure 3D, Suppl. Figure S2D). For example, 6-ketolithocholic acid concentrations were reduced, whereas concentrations of b-muricholic acid and taur-

a-muricholic acid were significantly elevated in *Bmal1^{SCN^{fl}/-}* mice (Figure 3D). Although other BAs measured had comparable concentrations in both genotypes, rhythmicity of various BAs was disrupted in *Bmal1^{SCN^{fl}/-}* including, 7-sulfocholic acid, ursodeoxycholic acid, taurocholic acid and allolithocholic acid (Figure 3E,F, Suppl. Figure S2D), suggesting altered fat and cholesterol metabolism [39].

Taken together, our results highlight the importance of the central clock in synchronizing peripheral clocks located in GI tissues. In addition, these results show for the first time loss of microbial taxa and their functional outputs, in particular SCFAs and BAs, in mice lacking central clock function, which associates with adiposity and impaired glucose metabolism in these animals [6].

3.4. Simulated shift work induces circadian desynchrony between GI clocks

Epidemiological and experimental studies indicate that frequent circadian desynchronization increases the risk of developing metabolic diseases and weight gain [40,41], similar to the phenotype observed in central clock-deficient mice [6]. Circadian desynchronization among tissue clocks, as observed in mice lacking the central clock [9], can be induced by misalignment between internal and environmental time, such as during jetlag or shift work [5]. To investigate whether shift work induces circadian desynchrony among GI clocks similar to the effects of a loss of central clock function in *Bmal1^{SCN^{fl}/-}* mice, wild type mice were exposed to phase shifts of 8 h every 5th day for 6–8 weeks to SSW (Figure 4A). The activity profiles gradually advanced during the first days in SSW (Figure 4A,B). In particular, in comparison to the LD profiles before SSW and the control cohort kept in LD, the activity onset advanced by less than 3 h at the 1st day (Figure 4A,B). This resulted in

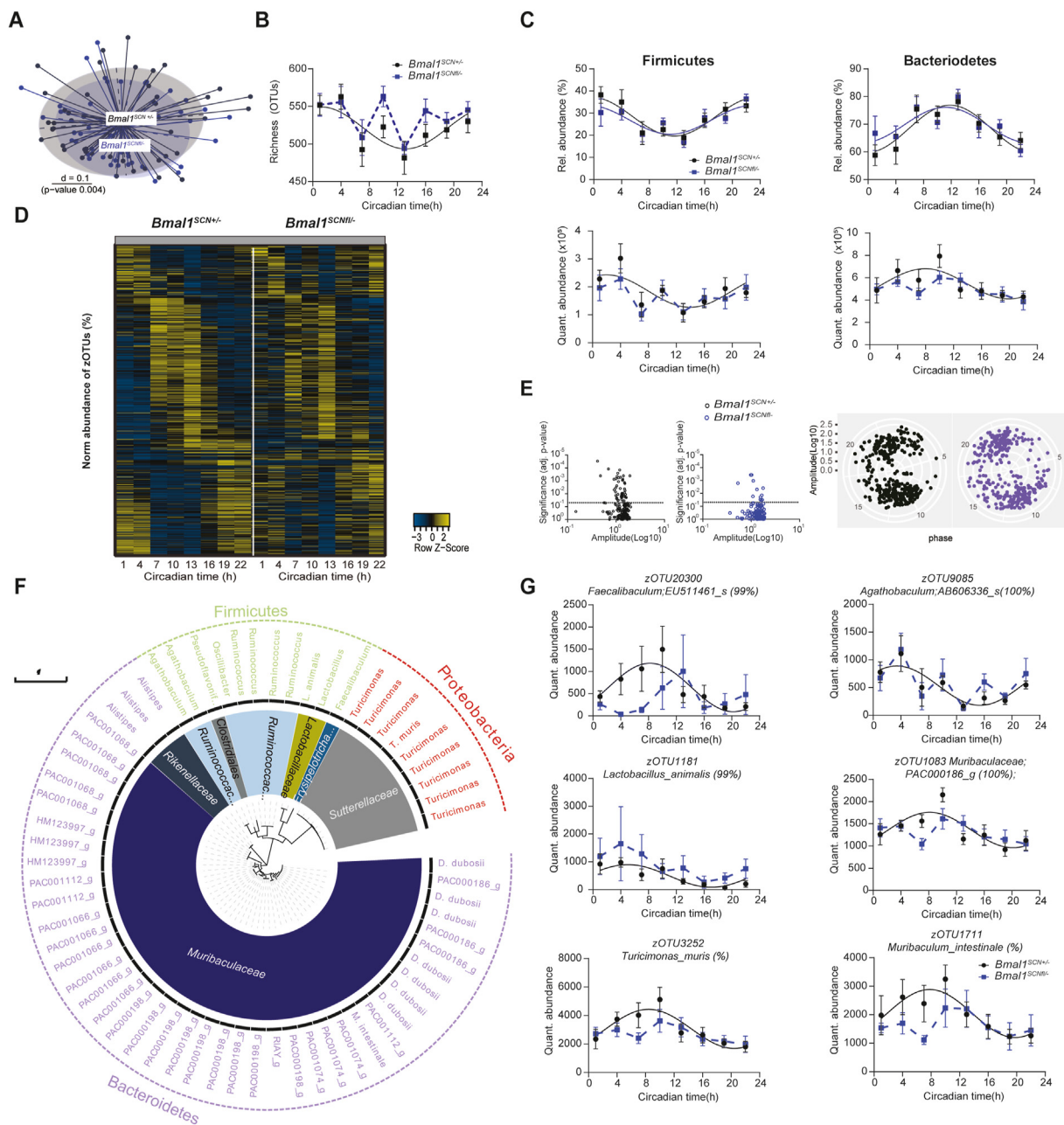


Figure 2: Disruption of microbiota rhythmicity in SCN-specific *Bmal1*-deficient mice (A) Beta-diversity MDS plot based on generalized UniFrac distances (GUniFrac) of fecal microbiota stratified by genotype. (B–C) Circadian profile of alpha diversity (B) and the relative and absolute abundance of major phyla (C). (D) Heatmap illustrating the relative abundance of 412 zOTUs (mean relative abundance >0.1%; prevalence >10%). Data are ordered based on the zOTUs phase in the controls and normalized based in the peak of each zOTU. (E) Significance and amplitude (based on JTK_CYCLE) of all zOTUs (left) and phase (based on cosine regression) distribution (right) in both genotype. Dashed line represent adj. p-value = 0.05 (JTK_CYCLE). (F) Taxonomic tree of zOTUs losing rhythmicity in *Bmal1*^{SCN^{-/-} mice based on quantitative analyses. Taxonomic ranks were indicated as phylum (outer dashed ring), families (inner circle) and genera (middle names). Each zOTU is represented by individual branches. (G) Circadian profiles of absolute abundance of example zOTUs losing rhythmicity in *Bmal1*^{SCN^{-/-} mice. Significant rhythms according to cosine-wave regression analysis (p-value ≤ 0.05) are visualized with a solid line, while data connected by dashed line indicate arrhythmicity. n = 6 mice/time point/genotype. Data are represented as mean ± SEM.}}

an equal distribution of activity between prior day and night, although total activity was unaffected (Figure 4B, Suppl. Figure S3A). In line with previous studies, mice in SSW significantly increased their body weight ($P < 0.0001$) [15] (Fig. 4C), although body fat composition and intestinal weight were undistinguishable from controls and no difference in food intake was found (Figure 4D, Suppl. Figure S4A-B) Next we thought to evaluate the functionality of the intestinal barrier, which can

influence the uptake of necessary nutrients (e.g. glucose) by measuring gut permeability. For example, increased intestinal permeability was previously correlated to metabolic syndrome (reviewed in [42]). Although colon permeability was slightly enhanced at CT13 during SSW, no difference was found between experimental groups (Figure 4E). Additionally, no difference in energy assimilation or total food intake was detected (Figure 4F).

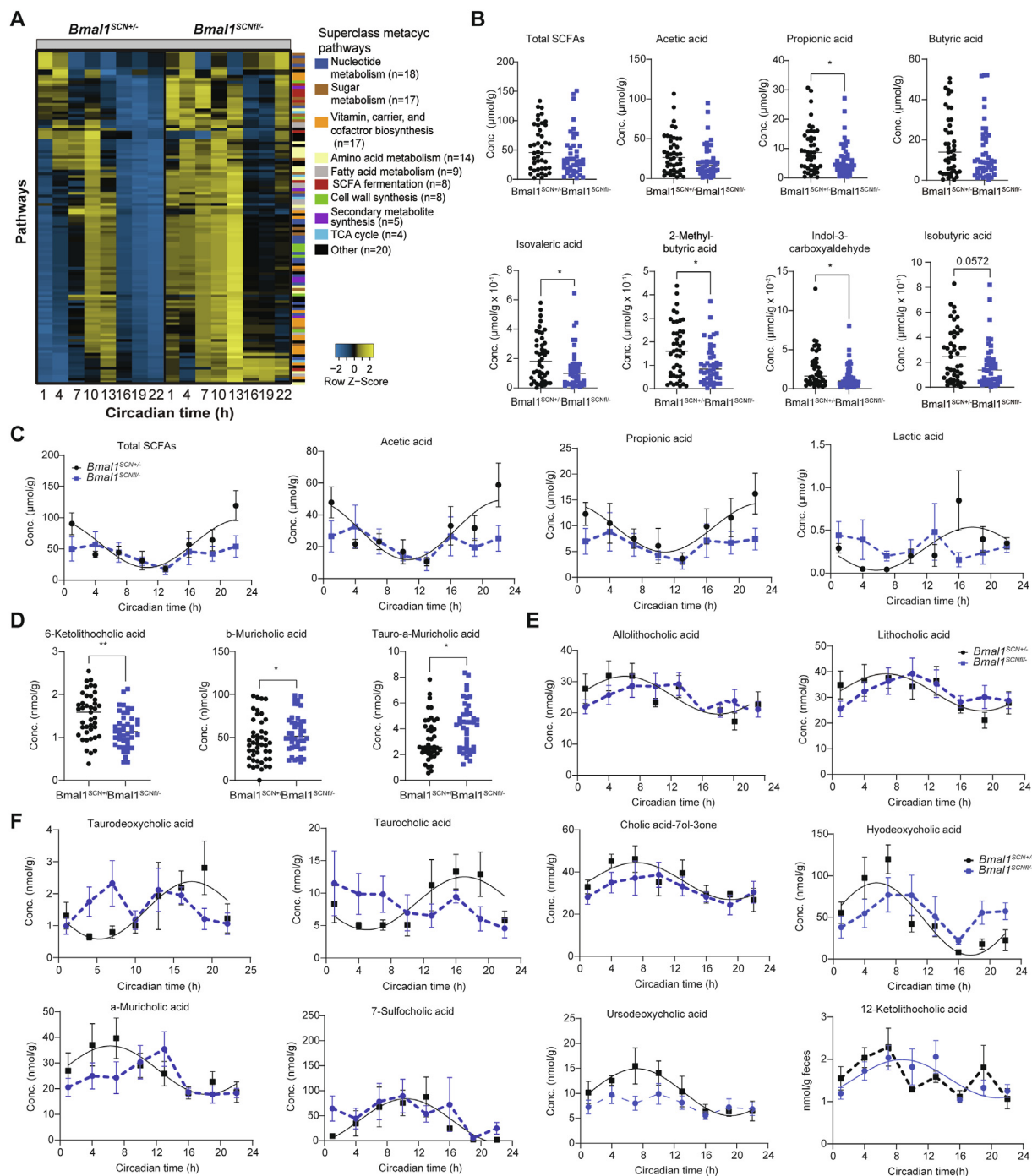


Figure 3: SCN clock-controlled microbial functions balance metabolic homeostasis (A) Heatmap representing MetaCyc Pathways predicted by PICRUST2.0 from zOTUs losing rhythmicity in *Bmal1^{SCN-/-}* mice. Pathways are ordered by the phase of the control and normalized to the peak abundance of each pathway. We color-coded the pathways according to their sub-classes. (B) Fecal SCFA concentrations in both genotype. (C) Circadian profiles of fecal SCFA. (D) Fecal bile acid concentrations in both genotype. (E–F) Circadian profiles of fecal bile acids. Significant rhythms according to cosine-wave regression analysis (p -value ≤ 0.05) are visualized with a solid line, while data connected by dashed line indicate arrhythmicity. Mann Whitney U test was used to assess concentration difference. $n = 6$ mice/time point/genotype. Data are represented as mean \pm SEM. Significance * $p \leq 0.05$, ** $p \leq 0.01$, *** $p \leq 0.001$, **** $p \leq 0.0001$.

Differences in the resetting speed of circadian clocks and between clock genes within the same tissue have been reported [5]. To test whether GI clocks are affected differentially by SSW, clock gene expression in GI tissues was measured at ZT1 and ZT13 (1 and 13 h after the lights on in controls). Indeed, diurnal expression of clock

genes in GI tissues and the liver as control was differentially affected at the 1st day during the last phase advance in SSW (Figure 4A,I, J). Although *Bmal1* and *Per2* in the liver, jejunum and proximal colon showed daytime dependent expression in both genotypes, *Dbp*, *Cry1* and *Rev-erb α* were affected only in specific tissues. For example, *Dbp*

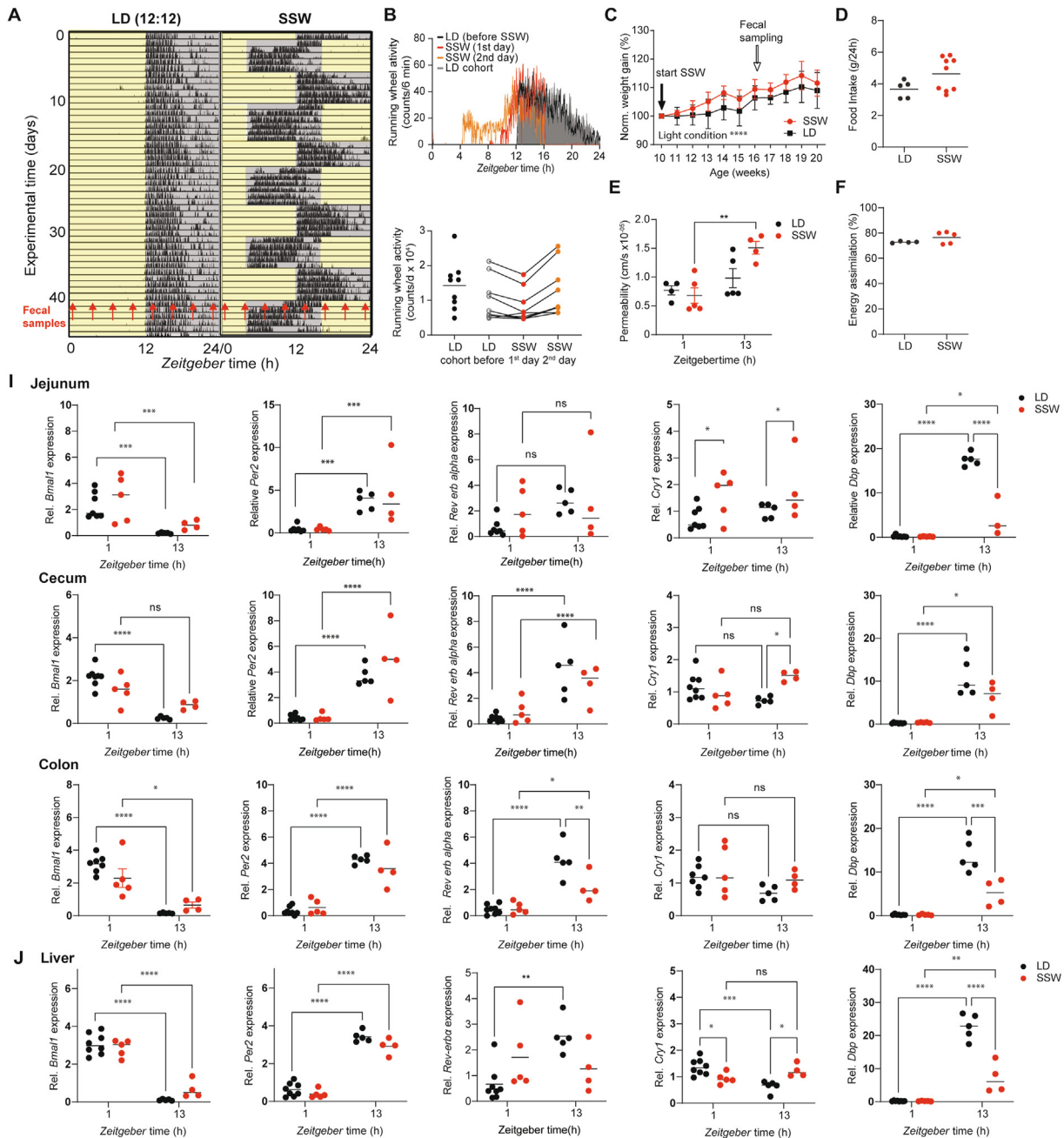


Figure 4: Simulated shift work induces circadian desynchrony between GI clocks (A) Representative actogram of a control mouse in 12-hour light/12-hour dark (LD) and under simulated shift work (SSW) condition. Tick marks represent running wheel activity. Yellow and grey shadings represent light and darkness respectively. Red arrows indicate fecal sample collection time points. (B) Diurnal total wheel-running activity profiles (top) and 24-h summary (bottom). (C) Normalized body weight gain of mice in SSW and LD condition. Total daily food intake (D), gut permeability (E) and energy assimilation (F). (I–J) Relative expression of core and accessory clock genes in GI tract (I) and liver (J) of WT mice in SSW (red) and their LD controls (black). N = 4–5 mice/time point/light condition. Data are represented as mean ± SEM. Mann Whitney U test was used to assess food intake and energy assimilation differences. Two-way ANOVA was used to assess the change in body weight and gene expression. Significance * $p \leq 0.05$, ** $p \leq 0.01$, *** $p \leq 0.001$, **** $p \leq 0.0001$.

was dramatically reduced at ZT13 in the liver and jejunum of mice exposed to SSW, whereas no daytime effect, but enhanced expression during SSW, was found for *Dbp* (Figure 4I,J). In contrast, in the cecum daytime differences of *Bmal1* were absent and *Cry1* significantly enhanced its expression at ZT13 during SSW, while *Per2*, *Rev-erb α* and *Dbp* were unaffected (Figure 4I). Moreover, in the colon of mice

undergoing SSW, a time difference in the expression of almost all clock genes examined (except of *Cry1*) was found, although *Bmal1*, *Rev-erb α* and *Dbp* expression was significantly suppressed at ZT13 (Figure 4I). These results indicate that all peripheral clocks examined were in different resetting stages of the phase advance and consequently circadian desynchronization was evident between GI clocks.

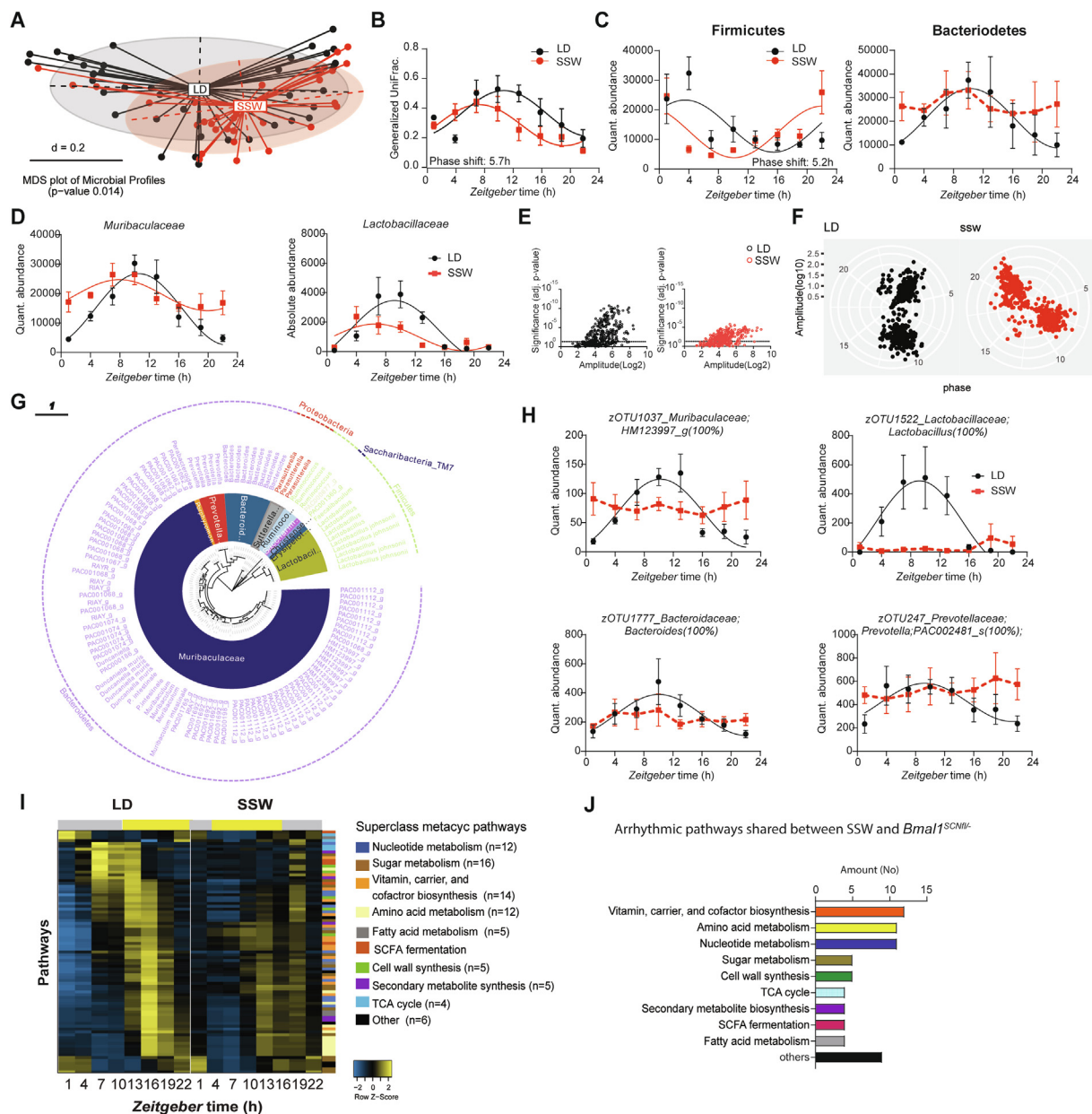


Figure 5: Simulated shift work disrupts rhythmicity of microbiota composition and function (A) Beta-diversity MDS plot based on generalized UniFrac distances (GUniFrac) of fecal microbiota stratified by light condition. (B) Circadian profile of generalized UniFrac distance normalized towards ZT1 of the controls. (C–D) Circadian profiles of the absolute abundance of major phyla (C) and families (D). (E) Significance and amplitude (based on JTK_CYCLE) of all zOTUs (E) and phase (based on cosine regression) distribution (F) in both genotype, dashed line represents adj. p -value = 0.05 (JTK_CYCLE). (G) Taxonomic tree of zOTUs losing rhythmicity in SSW based on quantitative analyses. Taxonomic ranks were indicated as phylum (outer dashed ring), then family (inner circle) and genera (middle names). Each zOTU is represented by individual branches. (H) Circadian profiles of absolute abundance of example zOTUs losing rhythmicity in SSW. (I) Heatmap representing MetaCyc Pathways predicted by PICRUST2.0 from zOTUs losing rhythmicity in SSW. Pathways are ordered by the phase of the control and normalized to the peak abundance of each pathway. We colored the pathways according to their sub-classes. (J) Bar chart representing the number of shared pathways losing rhythmicity in SSW and *Bmal1^{SCN1b}-* mice. Significant rhythms according to cosine-wave regression analysis (p -value ≤ 0.05) are visualized with a solid line, while data connected by dashed line indicate arrhythmicity. Significant phase shifts ($p \leq 0.05$) are indicated with the number of hours of phase shift. $n = 4$ – 5 mice/time point/genotype. Data are represented as mean \pm SEM.

3.5. Simulated shift work disrupts rhythmicity of microbiota composition and function

Previous research, including from our own group, indicates that changes in environmental conditions can modify microbial community composition and cause arrhythmicity of specific taxa [15,17,43]. In accordance, we found significantly different fecal microbial communities between mice exposed to LD and SSW conditions ($p = 0.014$)

(Figure 5A). Rhythmicity of GUniFrac distance quantification as well as the relative and quantitative abundance of major phyla and families was phase shifted in line with the advanced behavioral rhythm (Figure 4A,B, Figure 5B–D, Suppl. Figure S3B,C). Importantly, the quantitative abundance of *Bacteroidetes* lost rhythmicity in SSW (Figure 5C). Heatmaps of bacterial abundances over the course of the 24-hour day illustrate phase advanced rhythms of zOTUs during SSW

independent of the analysis (Suppl. Figure S3D,E). Moreover, arrhythmicity was identified during SSW in ~50% of all rhythmic zOTUs in LD conditions, including *Lactobacillus*, *Ruminococcus* and *Odoribacter* (Figure 5E,G, Suppl. Figure S3DF, Suppl. Table S1). zOTUs which lost rhythmicity in quantitative and relative analyses included taxa belonging to *Eubacterium*, *Bacteroides* and *Ruminococcus* (Figure 5G,H, Suppl. Figure S3G, Suppl. Table S1). The phase of the remaining rhythmic zOTUs in SSW advanced by 3.7–6.4h, including the genera *Alistipes*, *Duncaniella*, *Roseburia*, *Oscillibacter* and the family *Lachnospiraceae*, (Figure 5F, Suppl. Figure S3D,F, Suppl. Table S1). Of note, the average abundance of arrhythmic zOTUs belonging to the *Ruminococcaceae* and *Muribaculaceae* families as well as the genus *Lactobacillus* significantly differed between SSW and LD conditions (Figure 5G, Suppl. Figure S3F) in accordance with results obtained from mice exposed to chronic jetlag or sleep deprivation [15,43–45].

To evaluate whether GI clock desynchronization during SSW might have induced similar disturbance of microbial oscillations as observed in mice with central clock disruption, we analyzed rhythmicity of the microbiome in mice undergoing SSW. Of note, overall microbiota composition was not comparable between these two experiments performed in different animal facilities (Suppl. Figure S3H). However, this is in accordance with frequent reports illustrating that the housing situation dramatically influences microbiota composition [46]. To consider microbiota function rather than composition, we performed PICRUST analysis of zOTUs which lost rhythmicity in SSW (Figure 5I). Their predicted functionality was then compared to results obtained from arrhythmic taxa identified in *Bmal1^{SCNIII}-* mice (Figure 3A, Figure 5I, Suppl. Figure S3I). Independent of the approach of inducing circadian desynchronization, disrupted rhythmicity and changes in abundance were found in pathways related to amino acids, fatty acids as well as sugar metabolism and SCFA fermentation (Figure 5J), suggesting a functional link between circadian microbiota regulation and GI physiology. Of note, comparison of pathways between environmental and genetic circadian disruption show that pathways related to cell wall synthesis as well as metabolism of fatty acids, nucleotide and SCFA lost rhythmicity in *Bmal1^{SCNIII}-* mice and in SSW condition (Suppl. Table S2). Of note few pathways remained rhythmic in SSW although they lost rhythmicity in *Bmal1^{SCNIII}-* mice.

3.6. Simulated shift work-associated microbiota promote weight gain and suppress GI clocks

In order to directly investigate the effect of SSW-induced arrhythmicity of the microbiome on the host, we performed cecal microbiota transfer from donor mice undergoing 6 weeks of SSW and controls kept in LD into germ-free (GF) wild type recipients (Figure 6A). Mice receiving SSW-associated microbiota significantly increased their body weight (Figure 6B), in line with observations following fecal microbiota transplantation from mice exposed to chronic jetlag [15]. Interestingly, 6 weeks after transfer, body weight as well as most organ weights were undistinguishable between recipients (Figure 6A–C), indicating that microbial alterations are temporary in rhythmic hosts. Of note, cecum weight was significantly increased and plasma glucose was slightly enhanced, whereas plasma triglycerides were unchanged following transfer with SSW associated microbiota (Figure 6C, Suppl. Figure S4C). Microbial derived products, especially SCFAs and BAs have been described to alter clock gene expression in GI tissues [47,48]. This prompted us to measure clock gene expression in recipients as well as in GF controls. Indeed, mice receiving SSW-associated microbiota showed altered GI clock gene expression 6 weeks after the transfer (Figure 6D). Although most clock genes

examined in the proximal colon fluctuated between daytimes independent of the genotype of the donor, *Per2* expression was highly suppressed at ZT13 and the daytime difference of *Rev-erba* expression in controls was absent in mice receiving SSW-associated microbiota (Figure 6D). Similarly, *Per2*, *Cry1* and *Dbp* expression in jejunum as well as *Per2*, *Rev-erba* and *Dbp* expression in cecum was suppressed at ZT13 in mice receiving SSW-associated microbiota. Dampened daytime differences in GI clock gene expression followed similar trends than observations made in donor mice exposed to SSW and in GF mice (Figure 4I, Figure 6D). These results suggest that the microbiome can at least partly transfer the GI clock phenotype from the donor to the host and thus directly impact GI physiology. In mice receiving SSW-associated microbiota, we then investigated the effect of clock gene suppression on clock-controlled genes related to glucose and fat metabolism, such as *Fabp2*, *Ifabp*, *Sglt1*, *Glut2* and *Pparγ* [49–51]. Indeed, in the jejunum, suppressed expression was found for *Fabp2* involved in lipid uptake [50], *Sglt1* and *Glut2* a regulator for glucose uptake [52,53]. In the colon, enhanced expression was found for *Ifabp*, which is involved in the transport and metabolism of fatty acids and was linked to weight gain in mice [51]. Additionally, transfer of SSW-associated microbiota increased expression of *Pparγ* a transcriptional regulator of glucose and lipid metabolism [49] (Figure 6F) and SCFAs were shown to modulate the metabolic state of the host through PPARs [54]. Altogether, these results demonstrate the physiological relevance of the GI clock-microbiome crosstalk, specifically for maintenance of the host's metabolic health.

4. DISCUSSION

Mice with central clock dysfunction were shown to develop a metabolic phenotype and desynchrony in peripheral clocks, such as the adrenal, the liver, the heart, the pancreas and eWAT [6,9]. In addition, we provide evidence that GI clocks desynchronize in the absence of a functional central clock. Moreover, we demonstrate that desynchronization among GI clocks also appears in wild type mice exposed to SSW conditions. Our results comply with alterations in colonic clock gene expression following chronic jet lag [15] and suggest that GI clock desynchrony is a common feature during circadian disruption. Of note, distinct sections of the GI circadian system responded differentially to circadian disturbances, which was evident in the genetic model and during environmentally induced circadian disruption. Considering previous research indicating a temporal phase gradient of clock gene rhythms along the gut cranio–caudal axis [55], the circadian response to circadian disturbance might differ between gut sections. However, 24-hour profiling of clock gene expression over multiple days would be necessary to compare the kinetics of resetting between intestinal tissue clocks in different models. Notably, environmental and genetic circadian disruption influence the feeding fasting cycles differently [6,56]. Our results in *Bmal1^{SCNIII}-* mice demonstrate arrhythmic food intake behavior upon release in DD (Fig. 1A), whereas in SSW the daily patterns of food intake continued to be rhythmic but with a shifted phase [56]. This is in accordance to the wheel running activity rhythms documented in our approach (Figure 4A,B). As feeding time represents the main *Zeitgeber* for peripheral clocks [57], differences in the food intake patterns in SCN-specific *Bmal1*-deficient mice compared to mice exposed to SSW could impact the intestinal clocks differently and thus might explain the differences in expression patterns of intestinal genes observed in these models.

Recently, we identified that GI clocks are important regulators of gut microbiota rhythmicity [17]. Previous research identified food intake timing to influence microbial rhythmicity in mice with a defective

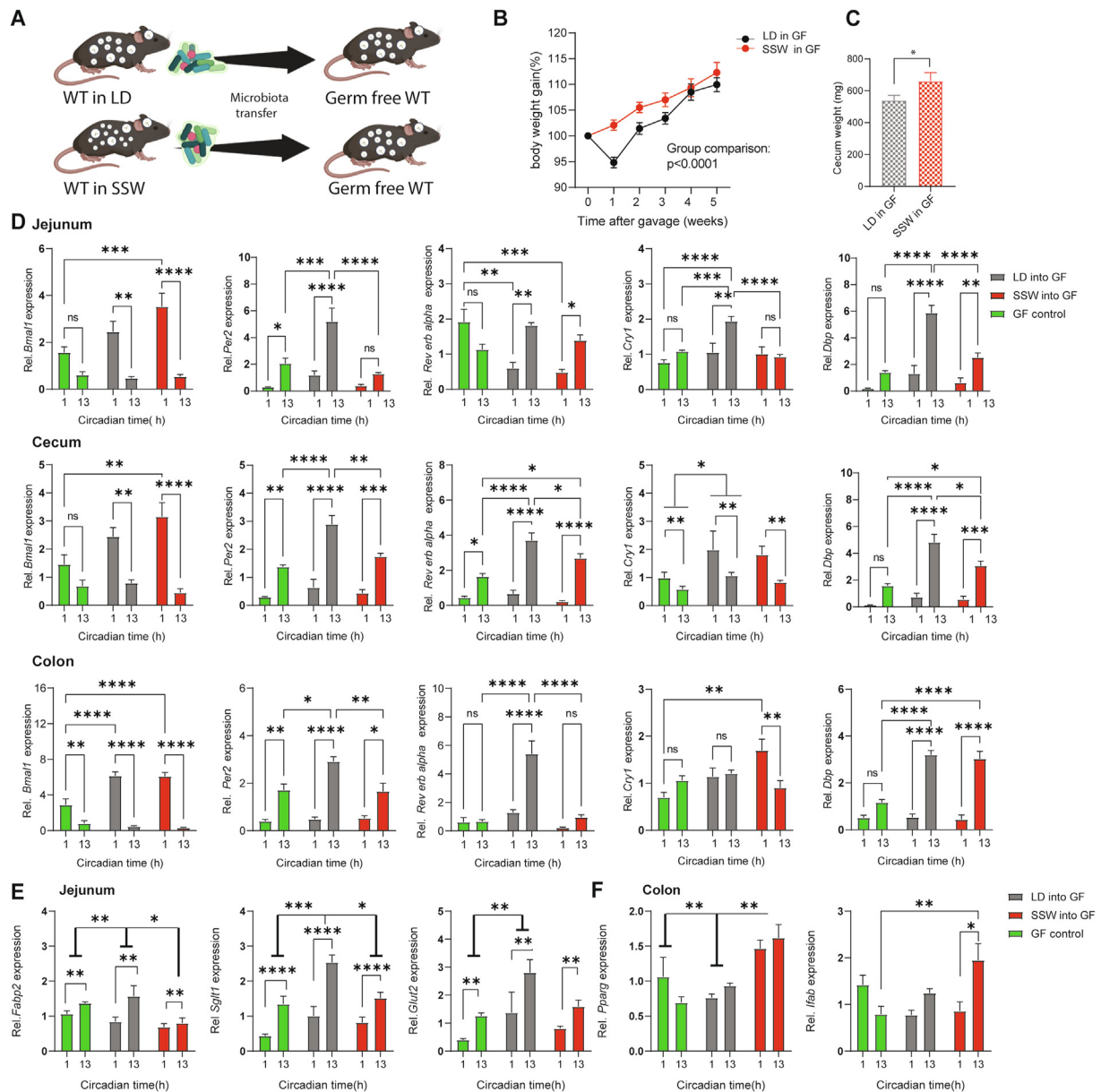


Figure 6: Simulated shift work-associated microbiota promote weight gain and suppress GI clocks (A) Schematic illustration of cecal microbiota transfer from SSW and LD donors (n = 4–5) into germ free wild type mice. (B) Normalized body weight gain of recipient mice. (C) bar chart illustrated cecum weight in recipient mice. (D–E) Relative expression at CT1 and CT13 of clock genes (D) and clock controlled gene (E, F) in the GI tract of germ free mice (green), germ free receiving SSW (red) and LD controls (black) microbiota. N = 5–6 mice/time point/light condition. Data are represented as mean \pm SEM. Mann Whitney U test was used to assess the different in cecum weight. Two-way ANOVA was used to assess the change in body weight and differences in gene expression. Significance * $p \leq 0.05$, ** $p \leq 0.01$, *** $p \leq 0.001$, **** $p \leq 0.0001$.

circadian system [15]. Consequently, arrhythmicity of the microbiota observed in mice with central clock disruption and in mice kept in SSW was likely induced by desynchronization among GI clocks or alteration of fasting-feeding behaviour or a combination of both. In line with recent results obtained from mice with dysfunctional intestinal clocks [17], taxa belonging to the families *Rikenellaceae*, *Ruminococcaceae* and *Muribaculaceae* as well as to the genera *Lactobacillus* and *Alis-tipes* lost rhythmicity in *Bmal1*^{SCN1f/-} mice and in mice undergoing SSW. Of note, disruption of rhythmicity was more severe in mice lacking a functional central clock. Here, arrhythmicity was found in microbial diversity and on the level of phyla and families. During SSW the abundance of the phylum *Bacteroidetes* and, thus, a substantial

amount of taxa remained rhythmic, although with an advanced phase. This discrepancy between both models might be explained by the accumulative effect of arrhythmic feeding behavior *Bmal1*^{SCN1f/-} mice (Fig. 1A), whereas in SSW the daily patterns of food intake were rhythmic but phase shifted [56]. Manipulating the timing of food intake has been shown to phase shift specific taxa belonging to *Alistipes*, *Lactobacillus* and *Bacteroides* [15,17]. Therefore, a phase-advanced food intake rhythm in SSW could have changed the phase of bacterial oscillations. Nevertheless, a substantial amount of taxa lost rhythmicity upon exposure to SSW and similarly in mice with SCN-specific and GI clock disruption [17], indicating that loss of synchrony between GI clocks during circadian disruption likely is

responsible for arrhythmicity of these taxa. Of note, few taxa sustained rhythmicity even during circadian disruption, which might be a result of altered but still functional peripheral clocks, or these taxa are driven by bacteria intrinsic factors.

Recently we discovered a link between microbiota rhythmicity, obesity and T2D development in humans [16], suggesting that microbial rhythms may play a causative role for disease development. Accordingly, transfer of microbiota from an obese human donor as well as from lean donors undergoing jetlag induces an obesity-associated phenotype in GF recipient mice [15,44,58]. However, these studies did not address whether obesity associated loss of microbial rhythmicity or general changes in abundance of bacteria are the underlying cause. Transfer experiments using mouse models with circadian dysfunction provide direct evidence for the physiological relevance of microbiota rhythms for metabolic health. For example, transfer of arrhythmic microbiota from gut-clock deficient mice disrupts GI homeostasis in recipient animals [17], and microbiota from mice exposed to environmentally induced circadian disruption promoting body weight gain in wild type mice. Similar results were obtained following microbiota transfer from jet lagged mice [15]. Together, these results suggest that on top of peripheral clock disruption in the fat and liver [6,9], the rhythmicity of the microbiome is a critical factor for the development of metabolic disease.

GI metabolism is strongly influenced by bacterially derived products, such as SCFAs and BAs [59,60]. After both genetic and environmental circadian disruption, loss of microbial rhythmicity was reflected by arrhythmicity of predicted microbial functionality, such as SCFA fermentation, as well as sugar, fatty acid and amino acid metabolism. Of note, loss of rhythmicity was more prominent on the level of pathways than on single zOTUs, indicating the involvement of oscillating zOTUs in multiple pathways. Targeted metabolite analysis further confirmed lack of rhythmicity of key microbial derived products in *Bmal1^{SCN1l}*- mice, namely SCFAs and BAs. For example, arrhythmicity was found for the SCFAs Propionic acid and Acetic acid. Both play a major role in fat and glucose metabolism and are capable in preventing diet induced obesity and insulin resistance [38]. Additionally, alterations in either rhythmicity or abundance of taurine-conjugated bile acids as well as the secondary BA Ursodeoxycholic acid were observed. These metabolites are known to impact signaling through the nuclear bile acid receptor FXR, resulting in the transcription of target genes important for lipid and glucose homeostasis (reviewed by [39]). Importantly, bacterial metabolites, such as SCFAs and BAs, are controlled by the circadian clock, and alterations in SCFA and BA oscillations were previously reported in mice exposed to chronic jet lag and in GI clock deficient animals [17,61]. Loss of rhythmicity of SCFAs as well as BAs which are both involved in sugar and fatty acid metabolism (reviewed by [62]) might alter metabolic functionalities of the host following circadian disruption, since both bacterial products are known to balance host metabolism (reviewed by [63]). In this regard, we previously reported an increased body weight gain, when *Bmal1^{SCN1l}*- mice were kept in DD for multiple weeks [6]. Of importance, loss of microbiota rhythms and subsequent microbial functions predominantly involved in glucose and lipid metabolism, such as Ursodeoxycholic acid, Propionic acid and Acetic acid [59,64,65], were already found at the 2nd day of DD and thus precede the obesity phenotype reported in these mice. Consequently, the observed microbial changes might represent an early event in the development of the metabolic phenotype of *Bmal1^{SCN1l}*- mice [6].

Importantly, shift work associated bacteria induced weight gain, slightly increased plasma glucose levels and directly affected the host's GI clock

function. In particular, GI clock dysregulation in donor mice following circadian disruption was partly reflected in recipients. For example, suppression of daytime differences in colonic *Rev-Erb α* and *Dbp* expression in jejunum was evident in both donor and recipient, indicating that microbiota transfer the circadian phenotype from the donor to recipients. Peripheral circadian clocks are known to control organ functions through regulation of tissue-specific CCGs ([4]). Accordingly, GI clock disruption in recipients altered the expression levels of CCGs in jejunum and colon, such as *Fabp2*, *Sglt1*, *Ifabp*, *Glut2* and *Ppar γ* , both involved in glucose and fat metabolism [49,52]. The mechanisms linking microbiota rhythms with functions of the GI tissue likely involve local epithelial–microbial interactions. Indeed, SCFAs and BAs have been reported to directly impact rhythmicity in intestinal epithelial cells and affect metabolic responses of the host [47,61,66,67]. Consequently, arrhythmicity of the transferred microbiota likely resulted in arrhythmicity of bacterial products, capable to alter GI clock function and, subsequently, metabolic CCGs. Therefore, our results provide first mechanistic insights into microbiota-dependent metabolic alteration during circadian disruption.

5. CONCLUSIONS

Taken together, the comparison of two models of genetic and environmentally induced circadian disruption revealed shared disruption at the level of GI clocks and identified microbial taxa and their functionalities involved in metabolic abnormalities of the host. Further, microbial alterations during SSW appear to be causal for the metabolic phenotype of the host. Our data provide first evidence that molecular alterations of GI clock function during circadian disruption are transferable between organisms through the microbiome. Thereby our data highlight the intestinal clock-bacteria dialogue as a potent underlying factor in the development of metabolic diseases in humans exposed to circadian disruption due to their lifestyle.

AUTHOR CONTRIBUTION

SK conceived and coordinated the project. BA, VP, MH, YN and EG performed mouse experiments and fecal samples collection. YN and MH measured epithelial membrane properties. MH conducted bomb calorimetry and NMR. SK and MH analyzed activity and food intake behavior. BA and MH performed 16S rRNA gene sequencing and bioinformatics analysis. BA analyzed gene expression, predicted microbial functionality and conducted germ free mouse colonization. KK, MG and BA performed targeted metabolomics and data analyses. SK supervised the work and data analysis. SK, HO and DH secured funding. BA, SK and MH wrote the manuscript. All authors reviewed and revised the manuscript.

FUNDING

SK was supported by the German Research Foundation (DFG, project KI 19,581) and the European Crohn's and Colitis Organisation (ECCO, grant 5280024). SK and DH received funding by the Deutsche Forschungsgemeinschaft (DFG, German Reuter Foundation) – Projektnummer 395357507 – SFB 1371). HO was funded by the DFG (project OS353-11/1).

DATA AVAILABILITY

Microbiota sequencing data and metabolite data will be available from the Sequence Read Archive (SRA) and the MetaboLights database for

Metabolomics experiments (<https://www.ebi.ac.uk/metabolights>) upon request.

ACKNOWLEDGEMENTS

The Technical University of Munich provided funding for the ZIEL Institute for Food & Health, animal facility support, technical assistance and support for 16S rRNA gene amplicon sequencing. Qu Guojing provided assistance with bomb calorimetry experiments and preliminary data collection. Živa Fras for providing technical support and assistance with animal handling.

DECLARATION OF COMPETING INTEREST

The authors declare no competing interests.

APPENDIX A. SUPPLEMENTARY DATA

Supplementary data to this article can be found online at <https://doi.org/10.1016/j.molmet.2022.101628>.

REFERENCES

- Mohawk, J.A., Green, C.B., Takahashi, J.S., 2012. Central and peripheral circadian clocks in mammals. *Annual Review of Neuroscience* 35:445–462.
- Oster, H., Damerow, S., Kiessling, S., Jakubcakova, V., Abraham, D., Tian, J., et al., 2006. The circadian rhythm of glucocorticoids is regulated by a gating mechanism residing in the adrenal cortical clock. *Cell Metabolism* 4(2):163–173.
- Lamia, K.A., Storch, K.F., Weitz, C.J., 2008. Physiological significance of a peripheral tissue circadian clock. *Proceedings of the National Academy of Sciences* 105(39):15172–15177.
- Zhang, R., Lahens, N.F., Ballance, H.J., Hughes, M.E., Hogenesch, J.B., 2014. A circadian gene expression atlas in mammals: implications for biology and medicine. *Proceedings of the National Academy of Sciences* 111(45):16219–16224.
- Kiessling, S., Eichele, G., Oster, H., 2010. Adrenal glucocorticoids have a key role in circadian resynchronization in a mouse model of jet lag. *The Journal of Clinical Investigation* 120(7):2600–2609.
- Kolbe, I., Leinweber, B., Brandenburger, M., Oster, H., 2019. Circadian clock network desynchrony promotes weight gain and alters glucose homeostasis in mice. *Molecular Metabolism* 30:140–151.
- Wendeu-Foyet, M.G., Menegaux, F., 2017. Circadian disruption and prostate cancer risk: an updated review of epidemiological evidences. *Cancer Epidemiology, Biomarkers & Prevention* 26(7):985–991.
- Marcheva, B., Ramsey, K.M., Peek, C.B., Affinati, A., Maury, E., Bass, J., 2013. Circadian clocks and metabolism. *Handb Exp Pharmacol* 217:127–155.
- Husse, J., Leliavski, A., Tsang, A.H., Oster, H., Eichele, G., 2014. The light-dark cycle controls peripheral rhythmicity in mice with a genetically ablated suprachiasmatic nucleus clock. *The FASEB Journal* 28(11):4950–4960.
- Turnbaugh, P.J., Ley, R.E., Mahowald, M.A., Magrini, V., Mardis, E.R., Gordon, J.I., 2006. An obesity-associated gut microbiome with increased capacity for energy harvest. *Nature* 444(7122):1027–1031.
- Karlsson, F.H., Tremaroli, V., Nookaew, I., Bergstrom, G., Behre, C.J., Fagerberg, B., et al., 2013. Gut metagenome in European women with normal, impaired and diabetic glucose control. *Nature* 498(7452):99–103.
- Qin, J., Li, Y., Cai, Z., Li, S., Zhu, J., Zhang, F., et al., 2012. A metagenome-wide association study of gut microbiota in type 2 diabetes. *Nature* 490(7418):55–60.
- Pedersen, H.K., Gudmundsdottir, V., Nielsen, H.B., Hyotylainen, T., Nielsen, T., Jensen, B.A., et al., 2016. Human gut microbes impact host serum metabolome and insulin sensitivity. *Nature* 535(7612):376–381.
- Thingholm, L.B., Ruhlemann, M.C., Koch, M., Fuqua, B., Laucke, G., Boehm, R., et al., 2019. Obese individuals with and without type 2 diabetes show different gut microbial functional capacity and composition. *Cell Host & Microbe* 26(2):252–264 e210.
- Thaiss, C.A., Zeevi, D., Levy, M., Zilberman-Schapira, G., Suez, J., Tengeler, A.C., et al., 2014. Transkingdom control of microbiota diurnal oscillations promotes metabolic homeostasis. *Cell* 159(3):514–529.
- Reitmeier, S., Kiessling, S., Clavel, T., List, M., Almeida, E.L., Ghosh, T.S., et al., 2020. Arrhythmic gut microbiome signatures predict risk of type 2 diabetes. *Cell Host & Microbe* 28(2):258–272 e256.
- Heddes, M., Altaha, B., Niu, Y., Reitmeier, S., Kleigrewe, K., Haller, D., et al., 2022. The intestinal clock drives the microbiome to maintain gastrointestinal homeostasis. *Nature Communications* 13(1):6068.
- Husse, J., Zhou, X., Shostak, A., Oster, H., Eichele, G., 2011. Synaptotagmin10-Cre, a driver to disrupt clock genes in the SCN. *Journal of Biological Rhythms* 26(5):379–389.
- Ubeda, C., Lipuma, L., Gobourne, A., Viale, A., Leiner, I., Equinda, M., et al., 2012. Familial transmission rather than defective innate immunity shapes the distinct intestinal microbiota of TLR-deficient mice. *Journal of Experimental Medicine* 209(8):1445–1456.
- Muller, V.M., Zietek, T., Rohm, F., Fiamoncini, J., Lagkouvardos, I., Haller, D., et al., 2016. Gut barrier impairment by high-fat diet in mice depends on housing conditions. *Molecular Nutrition & Food Research* 60(4):897–908.
- Clarke, L.L., 2009. A guide to Ussing chamber studies of mouse intestine. *American Journal of Physiology-Gastrointestinal and Liver Physiology* 296(6):G1151–G1166.
- Ussing, H.H., Zerahn, K., 1951. Active transport of sodium as the source of electric current in the short-circuited isolated frog skin. *Acta Physiologica Scandinavica* 23(2-3):110–127.
- Godon, J.J., Zumstein, E., Dabert, P., Habouzit, F., Moletta, R., 1997. Molecular microbial diversity of an anaerobic digester as determined by small-subunit rDNA sequence analysis. *Applied and Environmental Microbiology* 63(7):2802–2813.
- Subramanian, B., Gao, S., Lercher, M.J., Hu, S., Chen, W.-H., 2019. Evolvview v3: a webserver for visualization, annotation, and management of phylogenetic trees. *Nucleic Acids Research* 47(W1):W270–W275.
- Segata, N., Izard, J., Waldron, L., Gevers, D., Miropolsky, L., Garrett, W.S., et al., 2011. Metagenomic biomarker discovery and explanation. *Genome Biology* 12(6):R60.
- Reiter, S., Dunkel, A., Metwaly, A., Panes, J., Salas, A., Haller, D., et al., 2021. Development of a highly sensitive ultra-high-performance liquid chromatography coupled to electrospray ionization tandem mass spectrometry quantitation method for fecal bile acids and application on crohn's disease studies. *Journal of Agricultural and Food Chemistry* 69(17):5238–5251.
- Lagkouvardos, I., Fischer, S., Kumar, N., Clavel, T., 2017. Rhea: a transparent and modular R pipeline for microbial profiling based on 16S rRNA gene amplicons. *PeerJ* 5:e2836.
- Hughes, M.E., Hogenesch, J.B., Kornacker, K., 2010. JTK_CYCLE: an efficient nonparametric algorithm for detecting rhythmic components in genome-scale data sets. *Journal of Biological Rhythms* 25(5):372–380.
- Babicki, S., Arndt, D., Marcu, A., Liang, Y., Grant, J.R., Maciejewski, A., et al., 2016. Heatmapper: web-enabled heat mapping for all. *Nucleic Acids Research* 44(W1):W147–W153.
- Wirbel, J., Zych, K., Essex, M., Karcher, N., Kartal, E., Salazar, G., et al., 2020. Microbiome meta-analysis and cross-disease comparison enabled by the SIAMCAT machine-learning toolbox. *bioRxiv*, 2002.2006.931808.
- Segers, A., Depoortere, I., 2021. Circadian clocks in the digestive system. *Nature Reviews Gastroenterology & Hepatology* 18(4):239–251.
- Liang, X., Bushman, F.D., FitzGerald, G.A., 2015. Rhythmicity of the intestinal microbiota is regulated by gender and the host circadian clock. *Proceedings of the National Academy of Sciences* 112(33):10479–10484.

- [33] Tourlousse, D.M., Yoshiike, S., Ohashi, A., Matsukura, S., Noda, N., Sekiguchi, Y., 2017. Synthetic spike-in standards for high-throughput 16S rRNA gene amplicon sequencing. *Nucleic Acids Research* 45(4):e23.
- [34] Biddle, A., Stewart, L., Blanchard, J., Leschine, S., 2013. Untangling the genetic basis of fibrolytic specialization by lachnospiraceae and rumino-coccaceae in diverse gut communities. *Diversity* 5(3):627–640.
- [35] Gerard, P., 2013. Metabolism of cholesterol and bile acids by the gut microbiota. *Pathogens* 3(1):14–24.
- [36] Tian, B., Geng, Y., Wang, P., Cai, M., Neng, J., Hu, J., et al., 2022. Ferulic acid improves intestinal barrier function through altering gut microbiota composition in high-fat diet-induced mice. *European Journal of Nutrition* 61(7):3767–3783.
- [37] Douglas, G.M., Maffei, V.J., Zaneveld, J.R., Yurgel, S.N., Brown, J.R., Taylor, C.M., et al., 2020. PICRUSt2 for prediction of metagenome functions. *Nature Biotechnology* 38(6):685–688.
- [38] Lin, H.V., Frassetto, A., Kowalik Jr., E.J., Nawrocki, A.R., Lu, M.M., Kosinski, J.R., et al., 2012. Butyrate and propionate protect against diet-induced obesity and regulate gut hormones via free fatty acid receptor 3-independent mechanisms. *PLoS One* 7(4):e35240.
- [39] Dawson, P.A., Karpen, S.J., 2015. Intestinal transport and metabolism of bile acids. *Journal of Lipid Research* 56(6):1085–1099.
- [40] Qiao, H., Beibei, Z., Chong, T., Tieying, Z., Yuzhi, G., Jing, M., et al., 2020. Both frequency and duration of rotating night shifts are associated with metabolic parameters: a cross-sectional study. *Sleep Medicine* 71:89–96.
- [41] Parsons, M.J., Moffitt, T.E., Gregory, A.M., Goldman-Mellor, S., Nolan, P.M., Poulton, R., et al., 2015. Social jetlag, obesity and metabolic disorder: investigation in a cohort study. *International Journal of Obesity* 39(5):842–848.
- [42] Teixeira, T.F., Souza, N.C., Chiarello, P.G., Franceschini, S.C., Bressan, J., Ferreira, C.L., et al., 2012. Intestinal permeability parameters in obese patients are correlated with metabolic syndrome risk factors. *Clinical Nutrition* 31(5):735–740.
- [43] Bowers, S.J., Vargas, F., Gonzalez, A., He, S., Jiang, P., Dorrestein, P.C., et al., 2020. Repeated sleep disruption in mice leads to persistent shifts in the fecal microbiome and metabolome. *PLoS One* 15(2):e0229001.
- [44] Voigt, R.M., Forsyth, C.B., Green, S.J., Mutlu, E., Engen, P., Vitaterna, M.H., et al., 2014. Circadian disorganization alters intestinal microbiota. *PLoS One* 9(5):e97500.
- [45] Deaver, J.A., Eum, S.Y., Toborek, M., 2018. Circadian disruption changes gut microbiome taxa and functional gene composition. *Frontiers in Microbiology* 9:737.
- [46] Parker, K.D., Albeke, S.E., Gigley, J.P., Goldstein, A.M., Ward, N.L., 2018. Microbiome composition in both wild-type and disease model mice is heavily influenced by mouse facility. *Frontiers in Microbiology* 9:1598.
- [47] Tahara, Y., Yamazaki, M., Sukigara, H., Motohashi, H., Sasaki, H., Miyakawa, H., et al., 2018. Gut microbiota-derived short chain fatty acids induce circadian clock entrainment in mouse peripheral tissue. *Scientific Reports* 8(1):1395.
- [48] Leone, V., Gibbons, S.M., Martinez, K., Hutchison, A.L., Huang, E.Y., Cham, C.M., et al., 2015. Effects of diurnal variation of gut microbes and high-fat feeding on host circadian clock function and metabolism. *Cell Host & Microbe* 17(5):681–689.
- [49] Duszka, K., Picard, A., Ellero-Simatos, S., Chen, J., Defernez, M., Paramalingam, E., et al., 2016. Intestinal PPARgamma signalling is required for sympathetic nervous system activation in response to caloric restriction. *Scientific Reports* 6:36937.
- [50] Lau, E., Marques, C., Pestana, D., Santoalha, M., Carvalho, D., Freitas, P., et al., 2016. The role of I-FABP as a biomarker of intestinal barrier dysfunction driven by gut microbiota changes in obesity. *Nutrition & Metabolism* 13:31.
- [51] Lackey, A.I., Chen, T., Zhou, Y.X., Bottasso Arias, N.M., Doran, J.M., Zacharisen, S.M., et al., 2020. Mechanisms underlying reduced weight gain in intestinal fatty acid-binding protein (IFABP) null mice. *American Journal of Physiology-Gastrointestinal and Liver Physiology* 318(3):G518–G530.
- [52] Gouyon, F., Caillaud, L., Carriere, V., Klein, C., Dalet, V., Citadelle, D., et al., 2003. Simple-sugar meals target GLUT2 at enterocyte apical membranes to improve sugar absorption: a study in GLUT2-null mice. *The Journal of Physiology* 552(Pt 3):823–832.
- [53] Lehmann, A., Hornby, P.J., 2016. Intestinal SGLT1 in metabolic health and disease. *American Journal of Physiology-Gastrointestinal and Liver Physiology* 310(11):G887–G898.
- [54] Oh, H.Y.P., Visvalingam, V., Wahli, W., 2019. The PPAR-microbiota-metabolic organ trilogy to fine-tune physiology. *The FASEB Journal* 33(9):9706–9730.
- [55] Polidaro, L., Sotak, M., Sladek, M., Pacha, J., Sumova, A., 2009. Temporal gradient in the clock gene and cell-cycle checkpoint kinase Wee1 expression along the gut. *Chronobiology International* 26(4):607–620.
- [56] Zhong, L.X., Li, X.N., Yang, G.Y., Zhang, X., Li, W.X., Zhang, Q.Q., et al., 2019. Circadian misalignment alters insulin sensitivity during the light phase and shifts glucose tolerance rhythms in female mice. *PLoS One* 14(12):e0225813.
- [57] Damiola, F., Le Minh, N., Preitner, N., Kornmann, B., Fleury-Olela, F., Schibler, U., 2000. Restricted feeding uncouples circadian oscillators in peripheral tissues from the central pacemaker in the suprachiasmatic nucleus. *Genes & Development* 14(23):2950–2961.
- [58] Ridaura, V.K., Faith, J.J., Rey, F.E., Cheng, J., Duncan, A.E., Kau, A.L., et al., 2013. Gut microbiota from twins discordant for obesity modulate metabolism in mice. *Science* 341(6150):1241214.
- [59] Rios-Covian, D., Ruas-Madiedo, P., Margolles, A., Gueimonde, M., de Los Reyes-Gavilan, C.G., Salazar, N., 2016. Intestinal short chain fatty acids and their link with diet and human health. *Frontiers in Microbiology* 7:185.
- [60] Just, S., Mondot, S., Ecker, J., Wegner, K., Rath, E., Gau, L., et al., 2018. The gut microbiota drives the impact of bile acids and fat source in diet on mouse metabolism. *Microbiome* 6(1):134.
- [61] Desmet, L., Thijs, T., Segers, A., Verbeke, K., Depoortere, I., 2021. Chronodisruption by chronic jetlag impacts metabolic and gastrointestinal homeostasis in male mice. *Acta Physiologica* 233(4):e13703.
- [62] Nieuwdorp, M., Gijljamse, P.W., Pai, N., Kaplan, L.M., 2014. Role of the microbiome in energy regulation and metabolism. *Gastroenterology* 146(6):1525–1533.
- [63] Wahlstrom, A., Sayin, S.I., Marschall, H.U., Backhed, F., 2016. Intestinal crosstalk between bile acids and microbiota and its impact on host metabolism. *Cell Metabolism* 24(1):41–50.
- [64] Haase, S., Maurer, J., Duscha, A., Lee, D.H., Balogh, A., Gold, R., et al., 2021. Propionic acid rescues high-fat diet enhanced immunopathology in autoimmunity via effects on Th17 responses. *Frontiers in Immunology* 12:701626.
- [65] Fan, N., Meng, K., Zhang, Y., Hu, Y., Li, D., Gao, Q., et al., 2020. The effect of ursodeoxycholic acid on the relative expression of the lipid metabolism genes in mouse cholesterol gallstone models. *Lipids in Health and Disease* 19(1):158.
- [66] Segers, A., Desmet, L., Thijs, T., Verbeke, K., Tack, J., Depoortere, I., 2019. The circadian clock regulates the diurnal levels of microbial short-chain fatty acids and their rhythmic effects on colon contractility in mice. *Acta Physiologica* 225(3):e13193.
- [67] Govindarajan, K., MacSharry, J., Casey, P.G., Shanahan, F., Joyce, S.A., Gahan, C.G., 2016. Unconjugated bile acids influence expression of circadian genes: a potential mechanism for microbe-host crosstalk. *PLoS One* 11(12):e0167319.